Appl Phys B (2012) 108:553–558
DOI 10.1007/s00340-012-4971-3

Applied Physics B
Lasers and Optics

Broadband spectral conversion due to cooperative and phonon-assistant energy transfer from ZnO to Yb^{3+}

S. Ye · S. Tanabe · N. Jiang · D. Wang

Received: 1 December 2011 / Published online: 30 March 2012

Abstract The broadband spectral conversion from near-UV absorption into near-infrared emission around 1 μm is reported in the ZnO–$LiYbO_2$ hybrid phosphor, which is the benefit from the efficient energy transfer from ZnO to the Yb^{3+} ions that are specifically located at the interfacial diffusion regions between ZnO and $LiYbO_2$, rather than those in $LiYbO_2$ crystals. The Li^+-related and Yb^{3+}-related defect energy levels are formed inside the ZnO band gap in the ZnO–$LiYbO_2$ hybrid phosphor; the former act as the quenching centers for the excitons in ZnO and meanwhile the efficient energy donors for Yb^{3+} ions, and the latter are responsible for the red shift of ZnO visible emission when the excitation energy is lower than E_g. The excitation power dependence of Yb^{3+} emission intensities is measured to investigate the number of photons that are involved in the energy transfer process, which reveals that there are two channels for the sensitizing of Yb^{3+}: One is due to the energy transfer by the recombination of electrons and holes, which is a cooperative energy transfer process, and the other is via the energy feeding from the Li^+-related energy levels, which is a phonon-assistant energy transfer process.

S. Ye (✉) · D. Wang
School of Materials Science and Engineering, Tongji University, Shanghai 201804, China
e-mail: yesong@tongji.edu.cn
Fax: +86-21-88214392

S. Tanabe
Graduate School of Human and Environmental Studies, Kyoto University, Sakyo-ku Kyoto 606-8501, Japan

N. Jiang
Department of Physics, Arizona State University, Tempe, AZ 85287-1504, USA

1 Introduction

As a green, sustainable, and ubiquitous energy, the sunlight has been widely explored to alleviate the increasingly serious energy crisis since no other energy supply could be as plentiful as 120,000 terawatts provided by the sun [1]. At present, the majority of commercial solar cells are silicon based out of hundreds materials that have been considered, such as oxides, organic molecules, and polymers, due to its advantages of non-toxicity, stability, and abundance. However, it has not yet been an economic one due to the low energy conversion efficiency in the photovoltaic (PV) devices. Due to the mismatch between the solar spectrum and the spectral response of Si, much of the solar energy in UV and IR regions cannot be efficiently utilized. According to Shockley and Queisser's model, the theoretical efficiency limit for a single-junction solar cell with band gap of 1.1 eV is about 30 % [2]. One of the solutions to improve the PV conversion efficiency is to take full usage of the UV solar photons by "cutting" one incident UV or visible photon into two low-energy photons that can be effectively absorbed by silicon crystal [3–5].

Recently, the rare earth (RE) doped luminescent materials have been explored as spectral converters to improve the PV conversion efficiency of silicon solar cells [4]. It has been reported that the near-infrared quantum cutting in the RE^{3+}–Yb^{3+} (RE = Pr, Nd, Tb, Ho, Er, and Tm) co-doped luminescent materials may improve the PV conversion efficiency of silicon solar cells by spectral modification [6–13]. In these RE ions co-doped systems, the Yb^{3+}:$^2F_{5/2} \rightarrow {}^2F_{7/2}$ transition gives off a broadband emission around 1 μm, which corresponds to the maximum spectral response range of the crystal silicon PV devices. However, in these co-doped phosphors, the energy absorption is governed by the 4f–4f parity forbidden transitions of triva-

lent RE ions, in which only a small portion of the solar spectrum was involved in the spectral conversion process. This is a big drawback for practical application. Effectively harvesting the solar energy in a wide wavelength range is essential for ultimately enhancing the solar cell PV conversion efficiency. One effort has been made is to use RE ions with f–d transitions as the sensitizers for the Yb^{3+} ions, such as Ce^{3+} and Eu^{2+} [14–17]. Meanwhile, the silicon–oxygen-related defects with broadband absorption in the near UV region were also used as the energy donors for the Yb^{3+} in glassy materials [18, 19].

In this work, the direct band gap semi-conductor of ZnO was selected as the energy sensitizer for Yb^{3+} ions in the ZnO–$LiYbO_2$ hybrid phosphor, through which the broadband spectral conversion can be achieved due to the efficient energy transfer from ZnO to Yb^{3+}. The structural and spectroscopic measurements were carried out to systematically study the mechanism that is responsible for the energy transfer process, which indicates that there are two channels for the energy feeding of Yb^{3+} ions. As an environmental friendly phosphor that can effectively harvest the UV–visible solar photons in a broad wavelength region and convert them into the near-infrared emission around 1 μm, the ZnO–$LiYbO_2$ hybrid phosphor can be considered as a promising down conversion layer to enhance the PV conversion efficiency of silicon solar cells.

2 Experimental

The ZnO–$LiYbO_2$ hybrid phosphor was synthesized using the solid-state reaction method in a weak reducing atmosphere. The starting materials were high purity ZnO, Yb_2O_3, and Li_2CO_3. 1 mol% Yb_2O_3 and 1 mol% Li_2CO_3 were mixed first and grounded for 20 minutes, then added to ZnO. The mixtures were ground for 2 hrs, and sintered at 1050 °C for 2.5 hours by putting the crucible filled with raw materials into a bigger graphite crucible. For comparison, pure ZnO powder, ZnO mixed with 1 mol% Yb_2O_3 or 1 mol% Li_2CO_3 were sintered at the same conditions. The $LiYbO_2$ crystal was also prepared by sintering an equal molar percent of Li_2CO_3 and Yb_2O_3 mixture at 1050 °C for 2.5 hours in air. X-ray diffraction (XRD) profiles were obtained on a Rigaku D/MAX-RA diffractometer using a Cu target. The photoluminescence excitation (PLE) and photoluminescence (PL) measurements were carried out using a RF-5300PC (Shimadzu). The excitation power dependence of emission intensity was measured using a computer controlled measurement system including a xenon lamp (Asahi Spectra Co., Ltd., MAX-302), 350 and 400 nm band pass filters with bandwidth of 10 nm, a monochromator (Nikon, G250), a lock-in amplifier (NF Electronic Instruments LI-570A), and a Si photodiode (Electro-Optical System Inc., S-025-H).

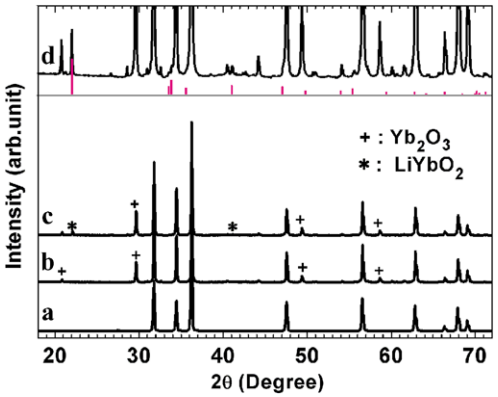

Fig. 1 X-ray diffraction patterns of (**a**) non-doped ZnO, (**b**) 1 mol% Yb_2O_3 mixed ZnO, (**c**) 1 mol% Li_2CO_3 and 1 mol% Yb_2O_3 co-mixed ZnO, and (**d**) the enlargement of (**c**) and the $LiYbO_2$ diffraction pattern (JCPDS #01-076-0428)

3 Results and discussion

3.1 Structure by XRD measurement

The XRD profiles of the sintered materials are shown in Fig. 1. In the non-doped ZnO, all the diffraction peaks belong to the hexagonal wurtzite ZnO. In the mixture of ZnO and Yb_2O_3, the diffraction peaks consist of both hexagonal ZnO and cubic Yb_2O_3, and there is no detectable change in the peak positions for ZnO, which indicates that the Yb^{3+} ions cannot be doped into the ZnO lattice by the solid-state reaction method. While in the Li_2CO_3 and Yb_2O_3 co-mixed ZnO, the new diffraction peaks belonging to $LiYbO_2$ phase were also observed, as shown in Figs. 1(c) and 1(d). According to our previous structural study [20], the $LiYbO_2$ crystals were grown on the ZnO surface with the formation of diffusion interfaces, and thereafter called ZnO–$LiYbO_2$ hybrid phosphor.

3.2 Origin of the intense Yb^{3+} emission

Figure 2 shows a group of PL spectra for the ZnO–$LiYbO_2$ hybrid phosphor under the excitation of 350–400 nm with a wavelength step of 10 nm. All of the PL spectra consists of a broadband visible emission and an infrared emission around 1 μm. The former is due to the radiative recombination of the electrons from the conduction band edge with deeply trapped holes in the ZnO [21, 22], and the latter is originated from the Yb^{3+}:$^2F_{5/2} \rightarrow {}^2F_{7/2}$ transition. Interestingly, the peak position of the visible emissions shows a red shift from 510 to 550 nm with the increase of excitation wavelength when the excitation energy is lower than the band gap of the ZnO semiconductor ($E_g \sim 3.37$ eV). The excitation wavelength dependence of the visible emission peak position is illustrated in the inset of Fig. 2.

The PLE spectra of these visible emissions at 510, 520, 540, and 550 nm, and the Yb^{3+} infrared emission at 986 nm

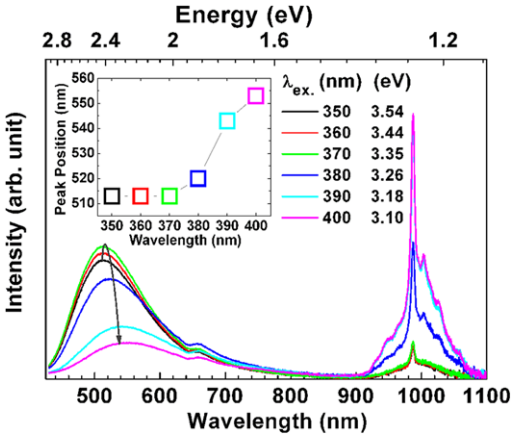

Fig. 2 PL spectra under the excitation of 350–400 nm with a wavelength step of 10 nm in the ZnO-$LiYbO_2$ hybrid phosphor. The *inset* shows the excitation wavelength dependence of ZnO visible emission peak position

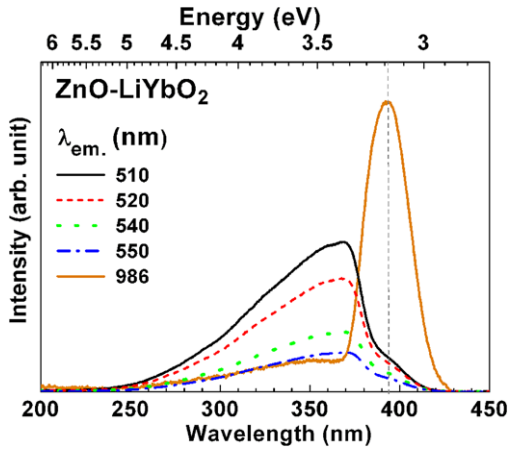

Fig. 3 PLE spectra of ZnO visible emissions at 510, 520, 540, and 550 nm, and Yb^{3+} infrared emission at 986 nm in the ZnO–$LiYbO_2$ phosphor

were measured, as shown in Fig. 3. The PLE spectra for the visible emissions show a similar spectral profile, which is composed of a broad band in the near UV region and a smooth edge around 395 nm. The PLE spectra for Yb^{3+} infrared emission also show a similar broadband structure in the near UV region, however, a sharp peak at 395 nm. The similarity of the broad excitation band in the near-UV region indicates the energy transition from ZnO to Yb^{3+}, however, the origin of the sharp excitation need to be a further investigation.

In order to get clear on the mechanism that is responsible for the strong Yb^{3+} infrared emission and the red shift of ZnO visible emission in the ZnO–$LiYbO_2$ hybrid phosphor, the PLE and PL spectra were also measured in the non-doped, 1 mol% Yb_2O_3 single-mixed and 1 mol% Li_2CO_3 single-doped ZnO, respectively. The results are given in Fig. 4. The PLE spectrum of the visible emission in the

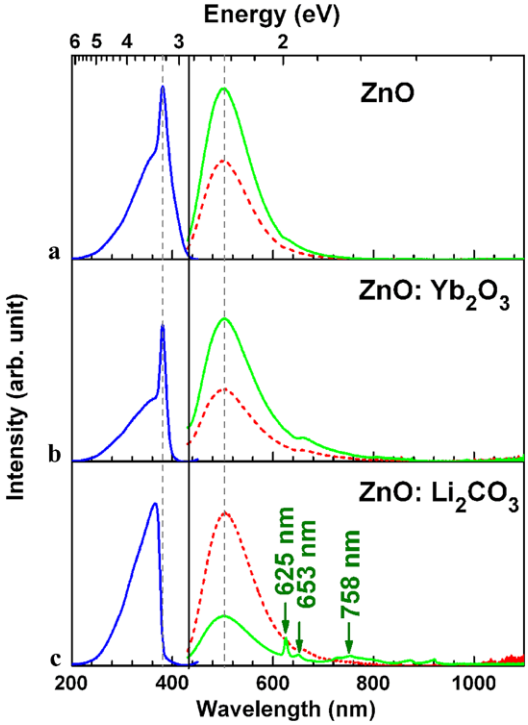

Fig. 4 PLE spectra of ZnO visible emission at 503 nm (*blue solid*), and PL spectra excited by 350 nm (*red dash*), and 380 nm (*green solid*) in (**a**) non-doped, (**b**) Yb_2O_3 single-mixed, and (**c**) Li_2CO_3 single-dope ZnO

non-doped ZnO consist of a broad band in the near-UV region and a sharp peak just below E_g, which are corresponding to the intrinsic absorption and excitonic absorption of ZnO, respectively [23, 24]. In the Yb_2O_3 single-mixed ZnO, only the visible emission from ZnO can be detected and the PLE spectrum of the visible emission shows similar spectral profile with that of the non-doped ZnO. In contrast, in the Li_2CO_3 single-doped ZnO sample, the sharp excitation band for the visible emission due to the excitonic absorption is annihilated. The quenching of the sharp excitation band for ZnO visible emission has also occurred in the ZnO–$LiYbO_2$ hybrid phosphor where the Li^+ ions are included; however, which is dominated in the Yb^{3+} excitation spectra.

As we know, the introduction of alien ions into a crystal lattice produces defects. In both the Li_2CO_3 single-doped ZnO and the ZnO–$LiYbO_2$ hybrid phosphor, the Li^+ ions may occupy substitutional and interstitial positions in the ZnO host, and thus the Li^+-related defect energy levels are formed in the band gap. The chemical defect formation due to Li^+-doping mainly occurs as follows [25–27]:

$$Li_2O \xrightarrow{ZnO} 2Li'_{Zn} + Li_i^{\bullet} + O_O^x$$

Based on the observations in Figs. 2–4, the Li^+-related defect energy levels may act as the quenching centers for the excitons in ZnO and meanwhile the energy donors for Yb^{3+} ions. It should be noticed that under the sub-band ex-

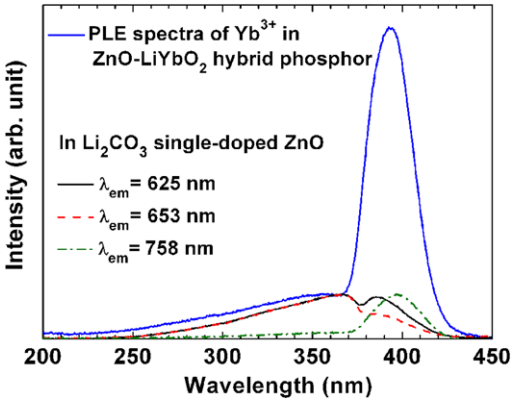

Fig. 5 PLE spectra of 625, 653, and 758 nm emissions in the Li_2CO_3 single-doped ZnO, which are normalized at the maximum intensity. The PLE spectrum of Yb^{3+} 986 nm emission in the ZnO–$LiYbO_2$ hybrid phosphor is also plotted here for comparing, which is normalized at the maximum of intrinsic absorption

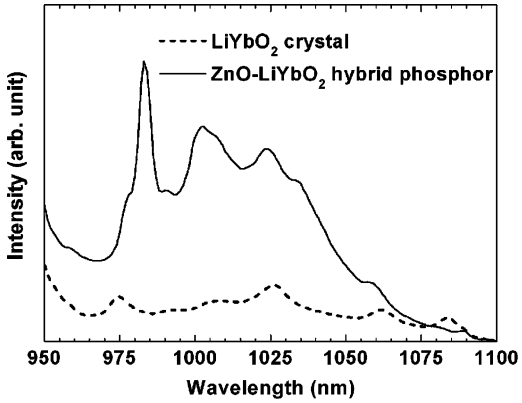

Fig. 6 Yb^{3+} PL spectra in the ZnO–$LiYbO_2$ hybrid phosphor and the $LiYbO_2$ crystal under the excitation of 937 nm LD

citation of ZnO at 380 nm (~3.26 eV), the emissions at 625, 653 and 758 nm specially appeared in the Li_2CO_3 single-doped ZnO, as shown in Fig. 4(c), which can be attributed to the radiative emissions from the Li^+-related defects. In the ZnO–$LiYbO_2$ hybrid phosphor, these Li^+-related defect emissions are completely quenched, as shown in Fig. 2, indicating the Li^+-related defect energy levels are very efficient energy donors for Yb^{3+} ions. Meanwhile, by comparing the PLE spectra for the Li^+-related defect emissions and Yb^{3+} emission in Fig. 5, we can observe that the Yb^{3+} PLE spectrum envelops both of the excitation bands for the Li^+-related defect emissions; this is another evidence for the energy transfer from the Li^+-related defect energy levels to Yb^{3+} ions.

Moreover, we suggest that the strong infrared emission in the ZnO–$LiYbO_2$ hybrid phosphor is due to the efficient energy transfer from ZnO to the small amount of Yb^{3+} ions that are incorporated in to ZnO lattice along with the Li^+ ions at the interfacial diffusion regions, rather than the Yb^{3+} ions in the $LiYbO_2$ crystals. This suggestion can be proved by comparing Yb^{3+} PL spectra in the ZnO–$LiYbO_2$ hybrid phosphor and the pure $LiYbO_2$ crystals under the direct excitation of Yb^{3+}:$^2F_{5/2}$ energy level. As shown in Fig. 6, under the excitation of 937 nm LD, the ZnO–$LiYbO_2$ hybrid phosphor shows intense Yb^{3+} infrared emission with the same spectral profile as indirectly excited ZnO with near-UV light (as shown in Fig. 2). In contrast, the $LiYbO_2$ crystal shows much weaker Yb^{3+} emission with different spectral profile. Because the structure of Yb^{3+} PL spectrum is sensitively related to the local crystal field, the comparison in Fig. 6 indicates that the intense infrared emission in the ZnO–$LiYbO_2$ hybrid phosphors is originated from the Yb^{3+} ions that are located at the interfacial diffusion region.

3.3 Shift of the ZnO visible emission peak position

Considering the incorporation of Yb^{3+} ions into ZnO lattice at the interfacial diffusion region, the Yb^{3+}-related defect energy levels may be formed close to the conduction band edge, which can shallowly trap electrons. Comparing the electrons from the conduction band, the radiative recombination of the electrons from the Yb^{3+}-related defect energy levels with the deeply trapped holes gives off lower-energy emission. As a result, when the excitation energy is lower than E_g, the lower the excitation energy, the higher probability of the electron to be trapped by the Yb^{3+}-related defect energy levels, therefore, the more the low-energy emission contributes to the overall visible emission. This leads to the red shift of the visible emission with the increase of excitation wavelength. While when the excitation energy is higher than E_g, the electrons can be excited deep into the conduction band, so that the visible emission is due to the radiative recombination of the electrons relaxed to the conduction band edge with the deeply trapped holes, which gives off higher-energy emission with constant value.

3.4 Two channels for the sensitizing of Yb^{3+} in the ZnO–$LiYbO_2$ hybrid phosphors

In order to investigate the number of photons that are involved in the energy transfer process, the excitation power dependence of Yb^{3+} emission intensity was studied under the excitation of intrinsic absorption of 350 nm and excitonic absorption at 400 nm, respectively, as shown in Fig. 7. The relationship between the emission intensity I and the excitation power P can be described as $I \propto P^n$, which means the fitted slopes in Log–Log scale indicates the number of photons that are involved in the energy transfer process, and the $n = 1$ for one phonon process and $n = 0.5$

for quantum cutting process [18, 28–30]. It can be observed from Fig. 7 that under the excitation of 350 and 400 nm the slope for excitation power versus Yb^{3+} emission intensity in Log–Log scale has a value of 0.59 and 0.89, respectively. We therefore suggest that there may be two channels for the energy sensitizing of Yb^{3+} ions, as schematically shown in Fig. 8. One channel is due to the energy transfer by the recombination of electrons and holes in ZnO, and the other is via the energy transfer from the Li^{+}-related defect energy levels. When the electrons were excited into the conduction band or the Yb^{3+}-related defect energy levels through intrinsic absorption, the recombination of electrons with deeply trapped holes will sensitize two Yb^{3+} ions simultaneously, which is a cooperative energy transfer process that leads to the "cutting" of one UV photon into two infrared photons. This suggestion is also reasonable from the energy point of view, as the recombination energy is around 2.3 eV, which is twice the energy of Yb^{3+}:$^2F_{5/2}$ excited state. While when the excitation energy is low, the excitons will be created in the ZnO host. The exciton annihilation energy trapped at the Li^{+}-related energy levels can excite one Yb^{3+}, this is a phonon-assistant energy transfer process.

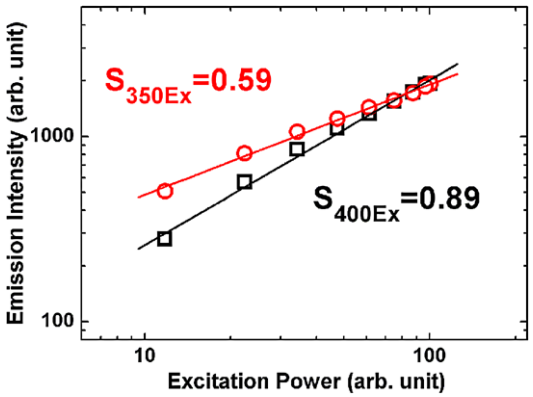

Fig. 7 Excitation power dependence Yb^{3+} infrared emission with the excitations of 350 and 400 nm, respectively

4 Conclusions

The ZnO–$LiYbO_2$ hybrid phosphor was synthesized by the solid state reaction in a weak reducing atmosphere, in which the broadband spectral conversion from near-UV to near-infrared can be achieved due to the efficient energy transfer from ZnO to those Yb^{3+} ions that are located at the interfacial diffusion region. Due to the introduction of Li^{+} ions and small amount of Yb^{3+} ions, the Li^{+}-related and Yb^{3+}-related defect energy levels were formed in the ZnO band gap. The former act as the quenching centers for excitons and meanwhile the efficient energy donors for the Yb^{3+} ions, while the latter are responsible for the red shift of ZnO visible emission when the excitation energy is lower than E_g. The excitation power dependence of emission intensity reveals that there are two mechanisms that are responsible for the energy transfer from ZnO to Yb^{3+}: the cooperative energy transfer process and the phonon assistant energy transfer process. This research revealed a new method to realize the broadband spectral conversion by selecting the direct band gap semi-conductor of ZnO as the energy sensitizer for Yb^{3+} ions, which may benefit the improvement of silicon solar cell PV conversion by spectral modification.

Acknowledgements This work was financially supported by the grant-in-aid program for young researchers of Kyoto-University Venture Business Laboratory, the JST PRESTO "Wavelength Conversion Material by Quantum Cutting toward Highly Efficient Photovoltaic Generation", the National Nature Science Foundation of China Nos. 50802083 and 51072133, and the Fundamental Research Funds for the Central Universities (No. 2011KJ018). One of the authors (S.Y.) would like to sincerely thank Professor Jacques Lucas from University of Rennes for all the valuable discussions and suggestions. The work at Arizona State University is supported by DOE award DE-FG52-09NA29451.

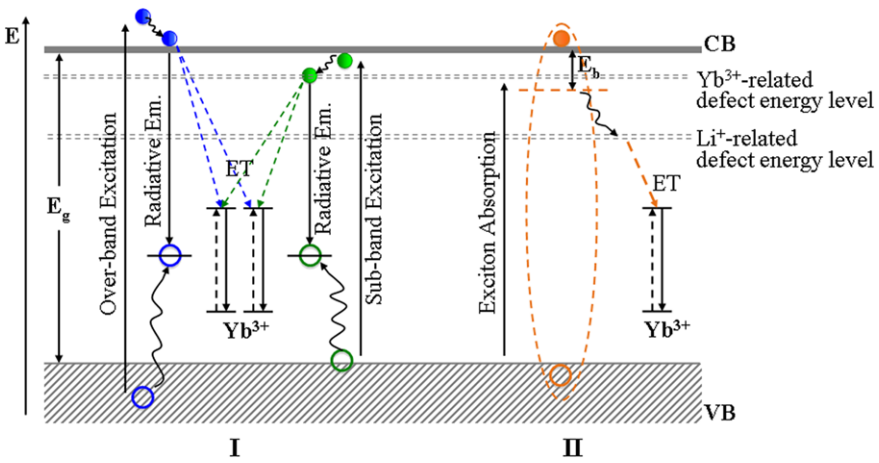

Fig. 8 Schematic diagrams that describing the energy transfer process from ZnO to Yb^{3+}: (I) the cooperative energy transfer process when sensitized by the recombination of electrons and holes. (II) The phonon assistant energy transfer process when sensitized by the Li^{+}-related defect energy level

References

1. O. Morton, Nature **443**, 19 (2006)
2. W. Shockley, H.J. Queisser, J. Appl. Phys. **32**, 510 (1961)
3. C. Strumpel, M. Mccann, G. Beaucarne, V. Arkhipov, A. Slaoui, V. Svrcek, C.D. Canizo, I. Tobias, Sol. Energy Mater. Sol. Cells **91**, 238 (2007)
4. B.M. van der Ende, L. Arats, A. Meijerink, Phys. Chem. Chem. Phys. **11**, 11081 (2009)
5. W. Shockley, H.J. Queisser, J. Appl. Phys. **32**, 510 (1961)
6. P. Vergeer, T.J.H. Vlugt, M.H.F. Kox, M.I. Den Hertog, J.P.J.M. Van der Eerden, A. Meijerink, Phys. Rev. B **71**, 0114119 (2005)
7. S. Ye, B. Zhu, J.X. Chen, J. Luo, J.R. Qiu, Appl. Phys. Lett. **92**, 141112 (2008)
8. S. Ye, B. Zhu, J. Luo, J.X. Chen, G. Lakshminarayana, J.R. Qiu, Opt. Express **16**, 8989 (2008)
9. Q.Y. Zhang, G.F. Yang, Z.H. Jiang, Appl. Phys. Lett. **91**, 051903 (2007)
10. X.F. Liu, Y.B. Qiao, G.P. Dong, S. Ye, B. Zhu, G. Lakshminarayana, D.P. Chen, J.R. Qiu, Opt. Lett. **33**, 2858 (2008)
11. L. Aarts, B.M. van der Ende, A. Meijerink, J. Appl. Phys. **106**, 023522 (2009)
12. D.Q. Chen, Y.L. Yu, H. Lin, P. Huang, Z.F. Shan, Y.S. Wang, Opt. Lett. **35**, 220 (2010)
13. H. Lin, D.Q. Chen, Y.L. Yu, A.P. Yang, Y.S. Wang, Opt. Lett. **36**, 876 (2011)
14. J.J. Zhou, Y.X. Zhuang, S. Ye, Y. Teng, G. Lin, B. Zhu, J.H. Xie, J. R Qiu, Appl. Phys. Lett. **95**, 141101 (2009)
15. J.J. Zhou, Y. Teng, S. Ye, Y.X. Zhuang, J.R. Qiu, Chem. Phys. Lett. **486**, 116 (2010)
16. J. Ueda, S. Tanabe, J. Appl. Phys. **106**, 043101 (2009)
17. D.Q. Chen, Y.S. Wang, Y.L. Yu, P. Huang, F.Y. Weng, J. Appl. Phys. **104**, 116105 (2008)
18. S. Ye, B. Zhu, Y. Teng, G. Lakshminarayana, X.P. Fan, J.R. Qiu, J. Appl. Phys. **105**, 063508 (2009)
19. S. Ye, B. Zhu, J. Luo, Y. Teng, J.X. Chen, G. Lakshminarayana, G.D. Qian, J.R. Qiu, Appl. Phys. Lett. **93**, 181110 (2008)
20. S. Ye, N. Jiang, F. He, X.F. Liu, B. Zhu, Y. Teng, J.R. Qiu, Opt. Express **18**, 639 (2010)
21. A. Van Dijken, E.A. Meulenkamp, D. Vanmaekelbergh, A. Meijerink, J. Lumin. **90**, 123 (2000)
22. A. Van Dijken, E.A. Meulenkamp, D. Vanmaekelbergh, A. Meijerink, J. Lumin. **87–89**, 454 (2000)
23. S. Shionoya, W.M. Yen, *Phosphor Handbook* (CRC Press, Boca Raton, 1998)
24. J.F. Muth, R.M. Kolbas, A.K. Sharma, S. Oktyabrsky, J. Narayan, J. Appl. Phys. **85**, 7884 (1999)
25. M.G. Wardle, J.P. Goss, P.R. Briddon, Phys. Rev. B **71**, 155205 (2005)
26. S. Majumdar, P. Banerji, Superlattices Microstruct. **45**, 583 (2009)
27. A. Yavuz Oral, Z. Banu Bahsi, M. Hasan Aslan, Appl. Surf. Sci. **253**, 4593 (2007)
28. W. Strek, A. Bednarkiewicz, P.J. Deren, J. Lumin. **92**, 229 (2001)
29. J.J. Zhou, Y. Teng, X.F. Liu, S. Ye, X.Q. Xu, Z.J. Ma, J.R. Qiu, Opt. Express **18**, 21663 (2010)
30. Y. Teng, J.J. Zhou, X.F. Liu, S. Ye, J.R. Qiu, Opt. Express **18**, 9671 (2010)